Soft Matter

Accepted Manuscript

ROYAL SOCIETY OF CHEMISTRY

www.rsc.org/softmatter

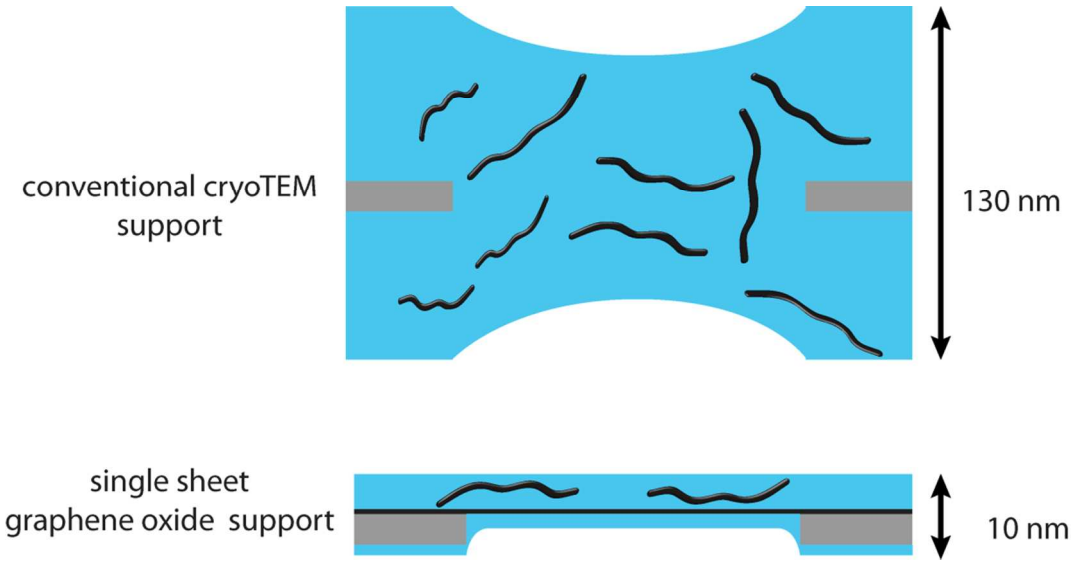

Text:

Ultra thin films prepared on single sheet graphene oxide substrates to enhance contrast and resolution in high resolution cryoTEM

Cite this: DOI: 10.1039/c0xx00000x

www.rsc.org/xxxxxx

ARTICLE TYPE

Graphene Oxide Single Sheets as Substrate for High Resolution cryoTEM

Marcel W.P. van de Put,[a,b,d] Joseph P. Patterson,[c] Paul H.H. Bomans,[a,b,d] Neil R. Wilson,[e] Heiner Friedrich,[a,b] Rolf A.T.M. van Benthem,[a,f] Gijsbertus de With,[a,b] Rachel K. O'Reilly,[c*] Nico A.J.M. Sommerdijk,[a,b,d*]

Received (in XXX, XXX) Xth XXXXXXXXX 20XX, Accepted Xth XXXXXXXXX 20XX
DOI: 10.1039/b000000x

CryoTEM is an important tool in the analysis of soft matter, where generally defocus conditions are used to enhance the contrast in the images, but this is at the expense of the maximum resolution that can be obtained. Here, we demonstrate the use of graphene oxide single sheets as support for the formation of 10 nm thin films for high resolution cryoTEM imaging, using DNA as an example. With this procedure, the overlap of objects in the vitrified film is avoided. Moreover, in these thin films less background scattering occurs and as a direct result, an increased contrast can be observed in the images. Hence, imaging closer to focus as compared with conventional cryoTEM procedures is achieved, without losing contrast. In addition, we demonstrate a ~1.8 fold increase in resolution, which is crucial for accurate size analysis of nanostructures.

Introduction

Transmission electron microscopy is a key technique in the characterization of both organic and inorganic nanostructures providing information on size, structure and morphology on the (sub)nanometer length scale.[1-6] For the TEM analysis of specimens dispersed in liquids, samples are conventionally dried from suspension onto a 30-50 nm carbon or polymer covered metal grid. For organic materials, which are relatively transparent to the electron beam, drying is often combined with negative staining to generate contrast. As both drying and the interaction with staining agents may affect the structure of the specimens under investigation, cryoTEM – which involves the vitrification of ~ 100-200 nm thin volumes of liquid – has evolved as an important technique for the visualization of nanostructures in their near native dispersed state.[7-10] However, to prevent radiation damage to the delicate specimens, cryoTEM is generally performed under low-dose conditions, which together with the often weak scattering of electrons in the vitrified solvent film, limits the resolution of the technique to the nanometer level. However, in a few cases high resolution images with sub-nanometer details[11, 12] or even lattice resolution have been reported.[13, 14] For dispersions of mechanically robust polymer-based nanoparticles – which do not compromise their structural integrity upon drying – it has been demonstrated that the use of graphene oxide supports, due to their low background signal, allowed for increased contrast and resolution of the suspended sample in conventional TEM imaging without the use of staining agents, thereby providing a convenient alternative for the more elaborate and infrastructurally more demanding use of cryoTEM.[15-17]

One limiting factor in cryoTEM is the thickness of the solvent layer; thinner layers lead to less scattering of the electrons due to the vitrified solvent, and therefore to increased contrast and higher resolution imaging of the sample. In addition, in the 2D analysis of nanometer-sized features a reduction of the film thickness will reduce the number of superimposed objects and, hence, lead to a more precise determination of their size and to a more reliable analysis of their shapes. Decreasing the film thickness, however, is limited by the size of the features in solution and the ability of the sample solution to form a mechanically robust freestanding film spanning the holes of the carbon support film, in particular for high surface tension liquids such as water.[18]

Graphene oxide (GOx), which is hydrophilic due to the presence of epoxy, hydroxyl, carbonyl and ether groups[19-21] and supersedes the more hydrophobic graphene in aqueous surface wetting behavior,[22-24] would be a potential robust low contrast layer to stabilize ultrathin aqueous films for high resolution cryoTEM imaging through favourable GOx-liquid interactions and simultaneous mechanical support. Here, we demonstrate the use of GOx to prepare and mechanically stabilize such ultrathin vitrified films suitable for high-resolution cryoTEM imaging of double strand DNA. The vitrified composite films (GOx + water) with a thickness of only ~10 nm, show unprecedented high electron transparency and prevent superimposition of the DNA in the film. The use of GOx further allowed us to introduce a more accurate focusing procedure using nanoprobe imaging (FEI settings) in combination with power spectrum analysis to determine the absolute defocus of the acquired images. This leads to more reliable imaging of low contrast objects, such as double strands DNA, in cryoTEM. Furthermore, the obtained contrast

enhancement can be used to image closer to focus, thereby

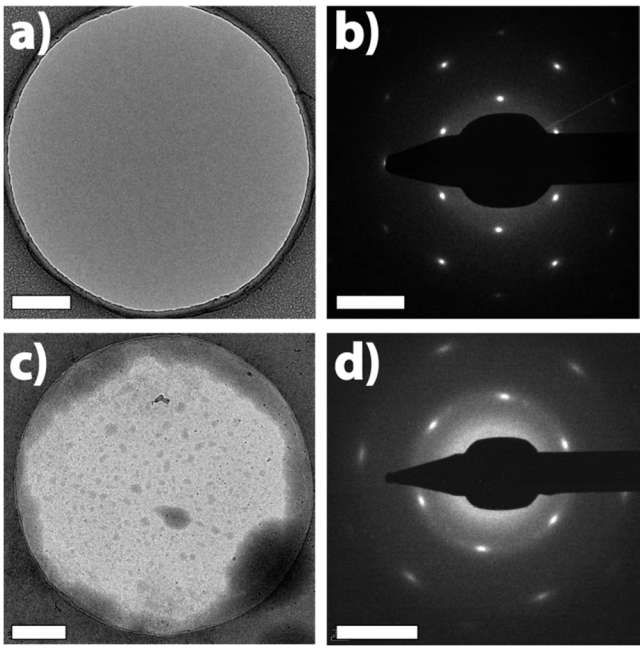

Fig. 1 Analysis of GOx monolayers. TEM images of graphene oxide sheets under (a) dry and (c) cryo-conditions with the corresponding electron diffraction patterns (b,d), respectively. Scale bars are 500 nm in (a,b) and 5 nm^{-1} in (c,d).

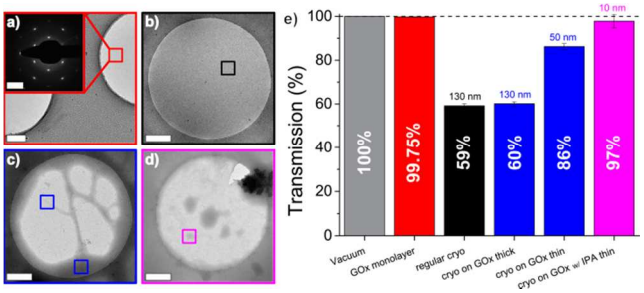

Fig. 2 Transmission measurements related to film thicknesses. (a) Dry and (b,c,d) CryoTEM images of aqueous films prepared on (b) a conventional TEM grid and (c,d) on graphene oxide substrates prepared with water and IPA/water vapors, respectively. (e) Thicknesses calculated from transmission measurements using an IMFP of 250 nm. The dashed line at 100% transmission (vacuum) is to guide the eyes. Scale bars are 500 nm in the cyoTEM images and 5 nm^{-1} in the inset in (a).

significantly increasing the resolution by a factor of ~1.8.

Results and discussion

Graphene oxide covered grids were prepared of which approximately 40% of the grid surface was covered with GOx monolayers (see Supplementary Information.[25, 26] By placing a 3 µL droplet of the aqueous analyte solution on these GOx-covered TEM grids and subsequent automated blotting using a vitrification robot (see Supplementary Information Figure S1†) thin vitrified water films were prepared on the TEM substrate.

The films were characterized using low-dose electron diffraction (LDED) to prevent crystallization of the water layer under the influence of the electron beam. The LDED patters showed a broadening of the diffraction spots due to scattering of the electrons by the vitrified water film (Figure 1).

To quantify the thickness of the vitrified water films, their electron transmission (I/I_0) was calculated from bright-field images (without energy filtering) using Lambert-Beer's law and the inelastic mean free path (IMFP) of the electrons (see Supplementary Information for details). The IMFP was calculated from the atomic inelastic cross-section, given the atomic numbers and the incident electron energy[27, 28] and amounted to 250 nm (see Supplementary Information Materials and Methods), a different value as may be expected from extrapolated data.[29] As the electron transmittance of a GOx monolayer amounted to 99.75%, it was neglected in the thickness calculations (Figure 2). For a regular cryoTEM sample the thickness of the vitrified water film was determined to be typically in the order of ~130 nm (I/I_0 = 59%). When water films were prepared on a GOx substrate, strong or extended blotting led to breaking of the films and subsequent dewetting of the GOx sheet. For example, the vitrification of a suspension containing silica nanoparticles after extensive blotting led to aqueous domains around these particles of ~50 nm (see Supplementary Information Figure S2†). Indeed, an intensity line scan shows a 1.3 fold increase in contrast as compared to conventional cryoTEM imaging. However, the observed dewetting process prevents complete spreading of the water film and hence hampers access to the increase in contrast required to obtain truly high resolution images. As this breaking of the water film can be attributed to the high surface tension of the water film, the addition of 2-propanol (isopropyl alcohol, IPA) was explored to lower the surface tension of the film.[30] Although this strategy minimizes the amount of 2-propanol that will infiltrate the sample, it is important to note that the addition of alcohols may dramatically influence the phase behaviour of soft matter, and thus adjustments in the procedure may be needed for different systems. To ensure this additive did not influence the solubility and/or integrity of the features under investigation, a strategy was chosen to minimize the contact time of the surface active agent with the specimen. In this approach the GOx grid was exposed to the vapour of an IPA/H2O mixture (20:80, v/v) for a duration of 24 seconds immediately prior to blotting and vitrification (see Supplementary Information for details). This led to a dramatic increase of the electron transmission of the vitrified layer up to 97% for most of the specimen, which corresponds to a vitrified ice layer thickness of only 10 nm (Figure 2).

To test the advantages of the ultrathin water films for cryoTEM imaging, specimens prepared from a 0.25 wt% solution of double strand salmon sperm DNA (~300 bp/molecule) were imaged at high magnification with both the regular cryoTEM method, as well as by using a GOx grid with the improved thin film procedure. Accurate analysis of specimens dispersed in liquids requires the identification and measurement of isolated particles in the cryo-TEM images. As individual nanoscale objects, such as DNA, are much thinner than the typical water layers formed in conventional cryoTEM, there is a high likelihood of overlap of individual particles and hence their superposition in the resultant images, as shown schematically in Figure 3. This complicates quantitative analysis of the images and reduces the confidence with which they can be interpreted. The significant reduction in

water film thickness on GOx thus gives an additional benefit; the chance of overlap is reduced so that the number of superimposed features that may complicate distinguishing individual objects are minimized. Hence, the images recorded from the GOx grid reveal the actual size and density of the DNA.

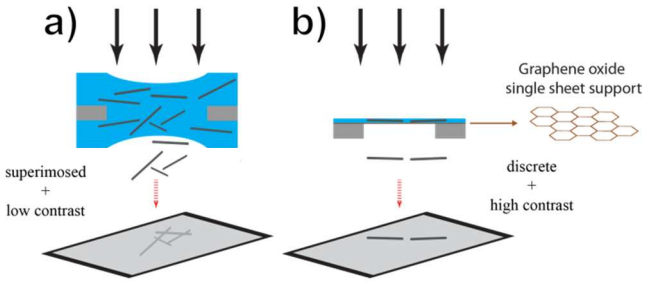

Fig. 3 Schematic representation of the effect of film thickness. (a) superimposed DNA in a vitrified film on a holey grid typically used in CryoTEM and (b) an ultra-thin water film with the same ribbons on a GOx monolayer support. The loss of contrast due to electron scattering and the projection of multiple ribbons make it more difficult to discriminate between individual particles in thicker films.

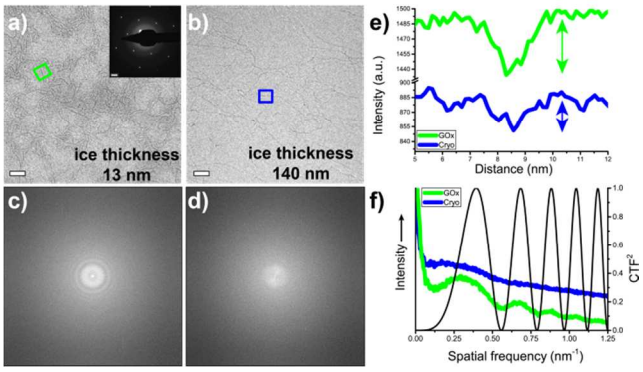

Fig. 4 Differences in contrast at −1600 nm defocus. CryoTEM images of DNA prepared on (a) a graphene oxide substrate (GOx) and (b) on a conventional TEM grid (Conv) with (c,d) the corresponding FFT's. To compare the images, the gray values are scaled to the background. The intensity profiles over DNA double strands (represented by boxes in (a) and (b)) are given in (e) to illustrate the contrast enhancement. The spectral density curves in (f) correspond to the calculated contrast transfer function (CTF) for the TU/e Titan operating at 300 kV at 61,000x magnification at −1600 nm defocus, with a spherical lens aberration of 2.7 mm. Scale bars are 20 nm.

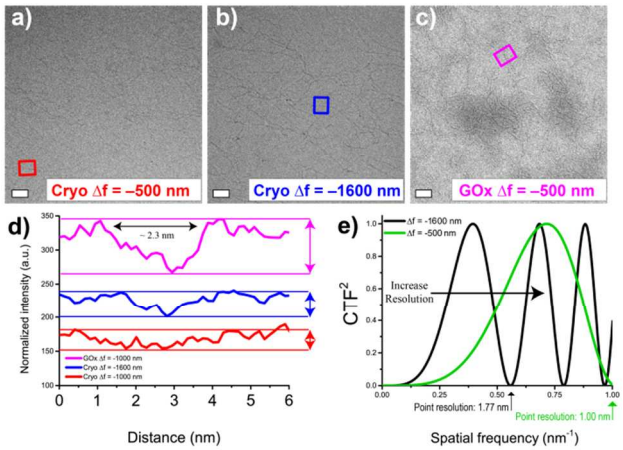

Fig. 5 Increase in resolution using smaller defocus. CryoTEM images of DNA prepared on a conventional cryoTEM support grid at (a) −500 nm defocus and (b) at −1600 nm defocus (see also Figure 4. (c) is the same sample prepared on a GOx monolayer substrate imaged at −500 nm. (d) shows that the contrast is lost in the conventional image upon decreasing defocus, while the contrast on the GOx substrate can still be used to identify the ribbons. The dashed lines are a guide to the eye. The CTF's plotted in (e) at −1600 nm and −500 nm defocus show the increase in resolution at lower defocus. Scale bars in (a-c) are 20 nm.

As Figure 4 shows, the thin film formation on GOx leads to immediate visible improvements in the quality of the images in terms of identifying discrete DNA duplexes. The reduction of the film thickness is beneficial for contrast enhancement, since fewer electron scattering events occur in the remaining water volume. The electron transmission in the thicker water pools on GOx, indicated by a higher background contrast, is at least 95%, corresponding to a film thickness of 13 nm. Intensity profiles across the DNA indeed show an 1.6 fold increase in contrast on GOx compared to conventional cryoTEM (Figure 4).

The reduced water film thickness is also beneficial for focusing. The relation between the reduction of the film thickness on GOx and the decrease in scattering events is also confirmed by the appearance of the easily recognizable Thon rings in the FFT's of the images and by the electron diffraction pattern in which no significant peak broadening could be observed. Distinction of the Thon rings is highly beneficial in the focusing procedure, since these patterns can be used to determine the actual defocus value of the imaged area.[31, 32] In regular low-dose protocols, the thick ice layer prevents effective use of the FFT's and one common strategy for focusing is by determining minimum contrast in an area 3-5 µm away from the acquisition area. Hence, the actual defocus value used for acquisition is established remotely from the imaging area and will be affected by the precise horizontal positioning of the grid with respect to the electron beam and the height differences in the sample surface, as well as the ability of the operator to determine the point of minimum contrast.[33, 34] Due to the clearly visible Thon rings in the FFT's of these GOx grids, a focused electron beam of 600 nm diameter ("nanoprobe mode") can be used in an area directly adjacent to the area of interest, leading to a negligible focus error while avoiding electron beam damage (see Supplementary Information for details).

Furthermore, the increase in contrast allows imaging closer to focus to obtain higher resolution images, since at lower defocus the contrast transfer function (CTF) oscillates less strongly and the first zero cross-over (point resolution) shifts to higher spatial frequencies (Figure 4d). Extending the region until the point resolution, i.e. where negative phase contrast occurs (scattering objects appear with dark contrast at negative defocus), is of paramount importance since this information is directly interpretable. In cryoTEM imaging, the loss of contrast prohibits imaging closer to focus and is thus limits the resolution that can be obtained. Lowering the absolute defocus value from −1600 to −500 nm results in a complete loss of contrast in conventional cryoTEM, while on the GOx grid the DNA can easily be identified (Figure 5). Here, the contrast is still higher than in the cryo-samples in Figure 3, but with the major advantage that at this defocus value the point resolution decreases to ~1 nm, significantly smaller than the dimensions of the DNA used.[35] Indeed, a line scan over an individual ribbon shows a width of 2.3 nm, in agreement with the literature.[36] Hence, this procedure does

not require a series of cryoTEM images at different focal values, from which the real dimensions can be determined by extrapolation of the measured values to zero defocus, a known method to correct for the interference of Fresnel fringes.[12, 13] This is not only beneficial for convenient size analyses of nanometer sized features in cryo-samples, but also reduces the amount of required data since less images have to be recorded and processed. Furthermore, the combination of avoiding object overlap, accurate focusing, and improved contrast allow high resolution single exposure imaging, which is crucial to obtain structural information from dispersions of unique objects, for which so-called single particle analysis (which involves the averaging of large numbers of images from identical copies as can be done for proteins[37, 38] or well defined synthetic objects[39]) is not an option.

Conclusions

With commercial high quality GOx grids becoming increasingly available, we have demonstrated how they can be used as support films for high-resolution single dose cryoTEM analysis of aqueous samples. In combination with the exposure to a low molecular weight alcohol (IPA) to reduce the surface tension of the solution, vitrified water films as thin as 10 nm could be obtained. These ultrathin films reduce the superposition of objects in the water layer, leading to more precise size and shape analysis, and the reduced electron scattering events increase the contrast of the embedded objects. The increase allows imaging closer to focus, leading to higher resolution images, improving the accuracy of size analysis. The use of GOx can further be used to apply a more reliable focusing method, which also enhances the accuracy of the size analysis of the imaged objects, particularly at dimensions close to 1 nm.

ACKNOWLEDGMENTS

The authors would like to thank K. Arapov for his help with the GOx solutions application and Dr. D. Chen for calculating the IMFP. This study was partly supported by DSM Ahead Materials Performance B.V., the Netherlands, the University of Warwick and the EPSRC, and by the Netherlands Organisation for Scientific Research (NWO) through a VICI grant to NAJMS.

Notes and references

[a] *Laboratory of Materials and Interface Chemistry, Eindhoven University of Technology, P.O. Box 513, 5600 MB Eindhoven, the Netherlands.*
[b] *Soft Matter Cryo-TEM Unit, Eindhoven University of Technology, P.O. Box 513, 5600 MB Eindhoven, the Netherlands..*
[c] *Department of Chemistry, Library Road, University of Warwick, Coventry, CV4 7AL, UK.*
[d] *Institute for Complex Molecular Systems, Eindhoven University of Technology, PO Box 513, 5600 MB, Eindhoven, The Netherlands.*
[e] *Department of Physics, University of Warwick, Coventry, CV4 7AL, UK.*
[f] *DSM Ahead Performance Materials B.V., P.O. Box 18, 6160 MD Geleen, the Netherlands.*
**E-mail: N.Sommerdijk@tue.nl; Rachel.OReilly@warwick.ac.uk*
† Electronic Supplementary Information (ESI) available: [defocus estimation, IMFP calculations]. See DOI: 10.1039/b000000x/

1. A. Bernecker, R. Wieneke, R. Riedel, M. Seibt, A. Geyer and C. Steinem, Journal of the American Chemical Society, 2009, 132, 1023-1031.
2. A. Blanazs, S. P. Armes and A. J. Ryan, Macromolecular Rapid Communications, 2009, 30, 267-277.
3. A. M. Caro, S. Armini, O. Richard, G. Maes, G. Borghs, C. M. Whelan and Y. Travaly, Advanced Functional Materials, 2010, 20, 1125-1131.
4. S. J. Holder and N. Sommerdijk, Polymer Chemistry, 2011, 2, 1018-1028.
5. T. Smart, H. Lomas, M. Massignani, M. V. Flores-Merino, L. R. Perez and G. Battaglia, Nano Today, 2008, 3, 38-46.
6. F. Wang, Y. Han, C. S. Lim, Y. Lu, J. Wang, J. Xu, H. Chen, C. Zhang, M. Hong and X. Liu, Nature, 2010, 463, 1061-1065.
7. H. Cui, T. K. Hodgdon, E. W. Kaler, L. Abezgauz, D. Danino, M. Lubovsky, Y. Talmon and D. J. Pochan, Soft Matter, 2007, 3, 945-955.
8. H. Friedrich, P. M. Frederik, G. de With and N. A. J. M. Sommerdijk, Angew Chem Int Edit, 2010, 49, 7850-7858.
9. F. Nudelman, G. de With and N. A. J. M. Sommerdijk, Soft Matter, 2011, 7, 17-24.
10. M. J. M. Wirix, P. H. H. Bomans, H. Friedrich, N. A. J. M. Sommerdijk and G. de With, Nano Lett, 2014, 14, 2033-2038.
11. E. M. Pouget, P. H. H. Bomans, J. A. C. M. Goos, P. M. Frederik, G. de With and N. A. J. M. Sommerdijk, Science, 2009, 323, 1455-1458.
12. W. J. E. M. Habraken, J. H. Tao, L. J. Brylka, H. Friedrich, L. Bertinetti, A. S. Schenk, A. Verch, V. Dmitrovic, P. H. H. Bomans, P. M. Frederik, J. Laven, P. van der Schoot, B. Aichmayer, G. de With, J. J. DeYoreo and N. A. J. M. Sommerdijk, Nat Commun, 2013, 4.
13. J. Baumgartner, A. Dey, P. H. H. Bomans, C. Le Coadou, P. Fratzl, N. A. J. M. Sommerdijk and D. Faivre, Nat Mater, 2013, 12, 310-314.
14. V. M. Yuwono, N. D. Burrows, J. A. Soltis and R. L. Penn, Journal of the American Chemical Society, 2010, 132, 2163-+.
15. R. S. Pantelic, J. C. Meyer, U. Kaiser, W. Baumeister and J. M. Plitzko, J Struct Biol, 2010, 170, 152-156.
16. J. P. Patterson, A. M. Sanchez, N. Petzetakis, T. P. Smart, I. I. I. T. H. Epps, I. Portman, N. R. Wilson and R. K. O'Reilly, Soft Matter, 2012, 8, 3322-3328.
17. J. Sloan, Z. Liu, K. Suenaga, N. R. Wilson, P. A. Pandey, L. M. Perkins, J. P. Rourke and I. J. Shannon, Nano Lett, 2010, 10, 4600-4606.
18. J. Dubochet and A. W. Mcdowall, J Microsc-Oxford, 1981, 124, Rp3-Rp4.
19. M. Hirata, T. Gotou, S. Horiuchi, M. Fujiwara and M. Ohba, Carbon, 2004, 42, 2929-2937.
20. A. Lerf, H. He, M. Forster and J. Klinowski, The Journal of Physical Chemistry B, 1998, 102, 4477-4482.
21. S. Stankovich, D. A. Dikin, G. H. B. Dommett, K. M. Kohlhaas, E. J. Zimney, E. A. Stach, R. D. Piner, S. T. Nguyen and R. S. Ruoff, Nature, 2006, 442, 282-286.
22. J. Rafiee, M. A. Rafiee, Z. Z. Yu and N. Koratkar, Adv Mater, 2010, 22, 2151-+.
23. J. P. Patterson, A. M. Sanchez, N. Petzetakis, T. P. Smart, T. H. Epps, I. Portman, N. R. Wilson and R. K. O'Reilly, Soft Matter, 2012, 8, 3322-3328.
24. B. C. Brodie, Quarterly Journal of the Chemical Society of London, 1860, 12, 261-268.
25. J. C. Meyer, A. K. Geim, M. I. Katsnelson, K. S. Novoselov, T. J. Booth and S. Roth, Nature, 2007, 446, 60-63.
26. N. R. Wilson, P. A. Pandey, R. Beanland, R. J. Young, I. A. Kinloch, L. Gong, Z. Liu, K. Suenaga, J. P. Rourke, S. J. York and J. Sloan, Acs Nano, 2009, 3, 2547-2556.
27. J. P. Langmore and M. F. Smith, Ultramicroscopy, 1992, 46, 349-373.
28. L. Reimer and H. Kohl, Transmission electron microscopy : physics of image formation, 5th edn., Springer, New York, NY, 2008.

29. M. Vulovic, R. B. G. Ravelli, L. J. van Vliet, A. J. Koster, I. Lazic, U. Lucken, H. Rullgard, O. Oktem and B. Rieger, J Struct Biol, 2013, 183, 19-32.
30. V. I. Kuchuk, I. Y. Shirokova and E. V. Golikova, Glass Phys Chem+, 2012, 38, 460-465.
31. F. Karimi Nejadasl, M. Karuppasamy, A. J. Koster and R. B. G. Ravelli, Ultramicroscopy, 2011, 111, 1592-1598.
32. M. Vulovic, E. Franken, R. B. G. Ravelli, L. J. van Vliet and B. Rieger, Ultramicroscopy, 2012, 116, 115-134.
33. M. Eibauer, C. Hoffmann, J. M. Plitzko, W. Baumeister, S. Nickell and H. Engelhardt, J Struct Biol, 2012, 180, 488-496.
34. L. M. Voortman, M. Vulovic, M. Maletta, A. Voigt, E. M. Franken, A. Simonetti, P. J. Peters, L. J. van Vliet and B. Rieger, J Struct Biol, 2014, 187, 103-111.
35. M. R. J. Vos, P. H. H. Bomans, F. de Haas, P. M. Frederik, J. A. Jansen, R. J. M. Nolte and N. A. J. M. Sommerdijk, Journal of the American Chemical Society, 2007, 129, 11894-+.
36. M. Mandelkern, J. G. Elias, D. Eden and D. M. Crothers, J Mol Biol, 1981, 152, 153-161.
37. R. Henderson, S. X. Chen, J. Z. Chen, N. Grigorieff, L. A. Passmore, L. Ciccarelli, J. L. Rubinstein, R. A. Crowther, P. L. Stewart and P. B. Rosenthal, J Mol Biol, 2011, 413, 1028-1046.
38. X. C. Bai, T. G. Martin, S. H. W. Scheres and H. Dietz, P Natl Acad Sci USA, 2012, 109, 20012-20017.
39. M. Kellermann, W. Bauer, A. Hirsch, B. Schade, K. Ludwig and C. Bottcher, Angew Chem Int Edit, 2004, 43, 2959-2962.